ACS OMEGA

http://pubs.acs.org/journal/acsodf

Article

Two-Dimensional V_2N MXene Monolayer as a High-Capacity Anode Material for Lithium-Ion Batteries and Beyond: First-Principles Calculations

Hongli Liu, Yongmao Cai,* Zhendong Guo, and Jing Zhou

Cite This: *ACS Omega* 2022, 7, 17756−17764

Read Online

ACCESS | Metrics & More | Article Recommendations

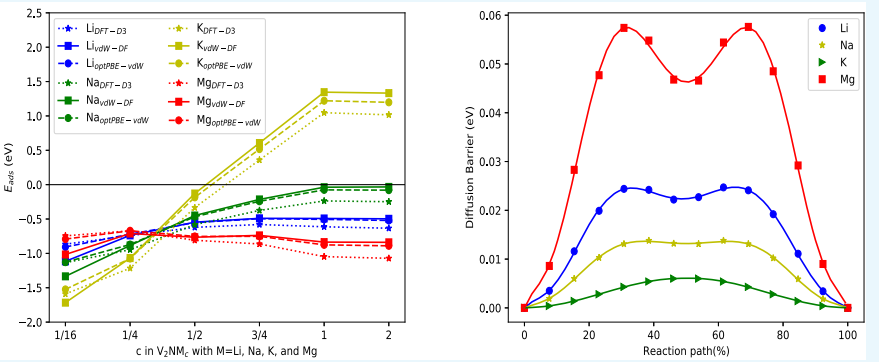

ABSTRACT: Two-dimensional metallic electrode materials with high energy density and excellent rate capability are crucial in rechargeable ion batteries. In this work, two-dimensional V_2N MXene monolayer has been predicted to be an attractive candidate anode material for rechargeable lithium, sodium, and magnesium ion batteries by first-principles calculations. We observe that V_2N monolayer is a metallic compound. The ion diffusion barriers on V_2N monolayer are predicted to be 0.025, 0.014, 0.004, and 0.058 eV for Li, Na, K, and Mg ions, respectively, which are rather low on the state-of-the-art two-dimensional energy storage materials. In addition, the calculated theoretical capacities of V_2N MXene monolayer are 925 mAh/g for Li ion, 463 mAh/g for Na ion, and 1850 mAh/g for Mg ion. The capacity of Li ions on V_2N monolayer is much higher than that of Li ions on the conventional anode graphite, and the extralarge capacity for Mg ions on V_2N monolayer is ascribed to the two-electron reaction and multilayer adsorption of Mg ions. Last, the average open circuit voltages of the V_2N MXene monolayer are also calculated to be 0.32 V for Li ions, 0.24 V for Na ions, and 0.34 V for Mg ions. These results provide a fundamental insight into electrochemical energy storage applications of two-dimensional V_2N MXene monolayer as a suitable candidate anode material for rechargeable Li, Na, and Mg ion batteries on the atomic scale.

1. INTRODUCTION

Rechargeable lithium-ion batteries (LIBs) have played an important role in the electrochemical energy storage devices since the first commercialization by Sony in 1991,[1] because of their high energy density, long cycling life, and lightweight design.[2] However, the large-scale application of LIBs has been hindered by high cost, safety issues, and limited Li reserves.[3,4] Therefore, batteries utilizing other metal ions are urgently needed. Compared with LIBs, rechargeable sodium-ion batteries (SIBs), potassium-ion batteries (PIBs), and magnesium-ion batteries (MIBs) have received much attention due to their abundant source, low cost, and operational safety.[5−8] Nevertheless, a bottleneck for practical applications of these batteries is the lack of high-performance electrode materials. For example, graphite, which is the most commonly used anode for LIBs, is not suitable in SIBs because of the extremely low capacity (35 mAh/g) caused by the weak interaction between Na and C atom.[9,10] Multivalent rechargeable ion batteries based on Mg^{2+} ions could provide higher capacity compared with monovalent ion batteries, however, they have poor mobility due to the stronger electrostatic interactions in solids and the polarization effect of divalent ions.[11,12]

Two-dimensional (2D) materials have attracted much attention in electrochemical energy storage because of their high specific surface area, adequate electrochemically active

Received: February 15, 2022
Accepted: May 4, 2022
Published: May 17, 2022

https://doi.org/10.1021/acsomega.2c00936
ACS Omega 2022, 7, 17756−17764

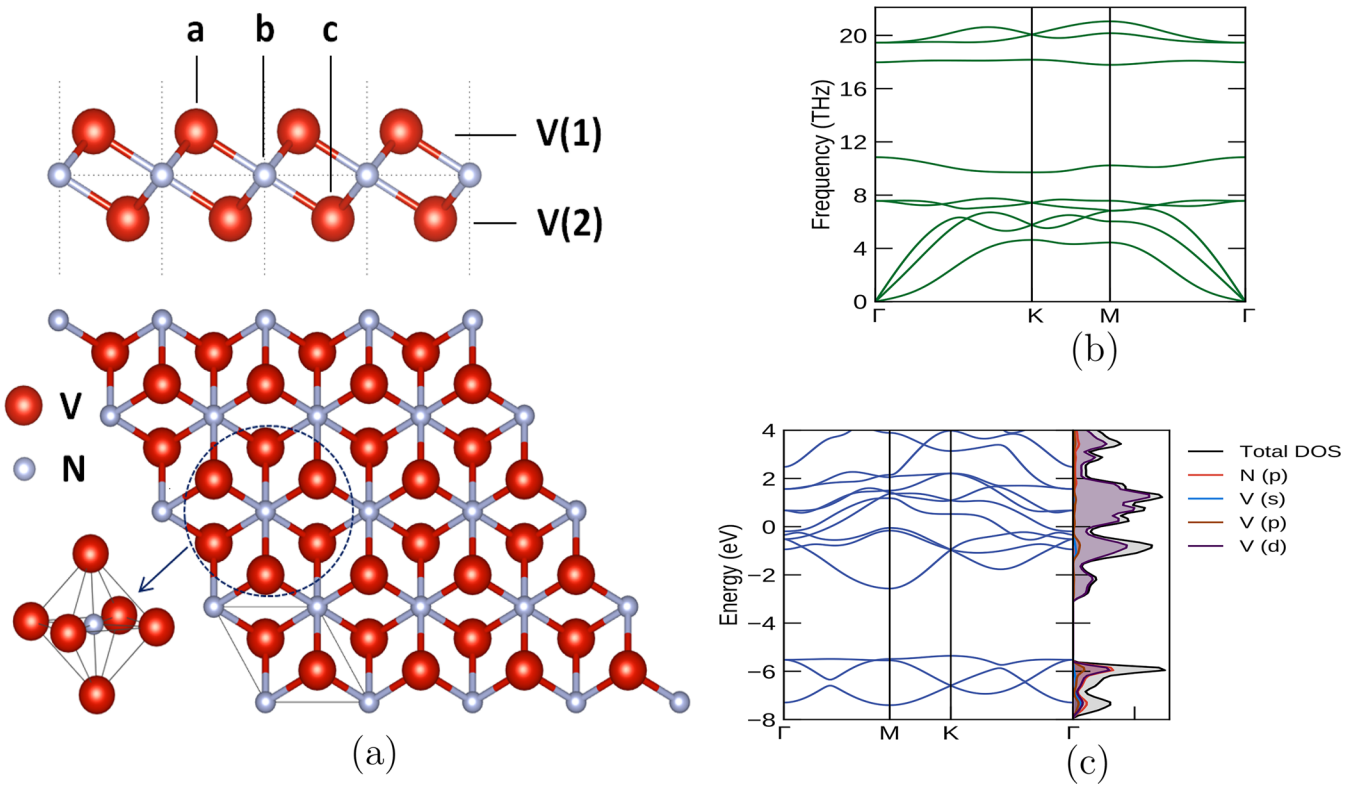

Figure 1. (a) Side and top views of the V_2N MXene monolayer, and the edge-shared octahedron structure of V_6N. a, b, and c represent the possible adsorption sites: top adsorption site, on top of V(1) atom in the first atomic layer; hcp adsorption site, on top of N atom in the second atomic layer; fcc adsorption site, on top of V(2) atom in the third atomic layer. (b) Calculated phonon dispersion and (c) band structure and density of state of V_2N monolayer.

sites and large interlayer space, which enhanced the capacities and mobilities.[13−15] Transition metal dichalcogenides, such as MoS_2, have a high theoretical capacity. However, the intrinsically poor electronic conductivity of MoS_2 seriously limits its electrochemical performance.[15] A new class of 2D transition-metal carbides/nitrides (so-called MXenes) with a general chemical formula $M_{n+1}X_n$, where "M" represents an early transition metal element and "X" refers to C, N, or their blends, are promising anode materials because of their good electrical conductivity, high rate performance, high capacity, and so forth.[16−18] Mashtalir et al. showed experimentally that Li ion capacity of $Ti_3C_2T_x$ nanosheets could reach 410 mAh/g with good rate capability.[19] Moreover, MXenes can be readily intercalated by a wide range of metal ions, such as Na, K, Mg, and Al ions, which is different from graphite.[20] As the synthesis of MXene is usually performed in aqueous solutions containing fluoride ions, the surface of the MXene layers are generally terminated with O, OH, or F.[21,22] Then, those metal ions' diffusion becomes more difficult with higher energy barriers because of these surface functional groups.[23,24] Significantly, these terminations can be altered or completely removed by postprocessing,[25,26] which has a profound effect on properties. Er et al. studied the energy storage of a variety of metal ions, including Li, Na, K, and Ca, on Ti_3C_2 MXene monolayers by first-principles calculations and revealed the cation storage mechanisms of MXenes on the atomic scale.[18] Recently, Wu et al. provided a fundamental insight into Ta_2CS_2 in the field of energy conversion and storage.[27]

Compared with the carbide and carbonitride MXenes, it is more difficult to synthesize nitride MXenes. In addition, the lower cohesive energy of $M_{n+1}X_n$ suggests the lower stability of the products after selective removal, which may lead to the products dissolution in the presence of hydrofluoric acid.[28] To date, only Ti_4N_3, Ti_2N, V_2N, MoN, and W_2N have been synthesized.[28−31] However, the study shows that it is feasible to transform the carbide MXenes into nitrides by high-temperature treatment in ammonia,[32] opening the door to chemical synthesis of 2D nitride MXenes. It should be noted that transition-metal nitrides provide higher conductivity than the corresponding carbides, which is desired in the battery applications.[33] Besides, vanadium-based materials with an abundance of compositions and crystal structures have gained increasing attention because of their high charge/discharge capacity arising from the multielectron redox chemistry of vanadium.[34]

First-principles calculation has been proved to be a powerful tool in studies of electrode materials in the rechargeable ion batteries. Zhou et al. evaluated some important indexes of the layered compounds in Materials Project database by database screening and DFT computations, and achieved over 20 kinds of layered electrode materials for multivalent batteries and some for SIBs, accelerating the development of battery materials..[35,36] In this work, we have systematically investigated the physical and electrochemical properties of V_2N MXene monolayer by first-principles calculations, including structural and electronic properties, ions diffusion barriers, theoretical specific capacities, and open circuit voltage (OCV) of V_2N monolayer as electrode materials for LIBs and beyond. Our studies revealed that 2D V_2N is an ideal candidate anode material for electrochemical energy storage applications.

https://doi.org/10.1021/acsomega.2c00936
ACS Omega 2022, 7, 17756−17764

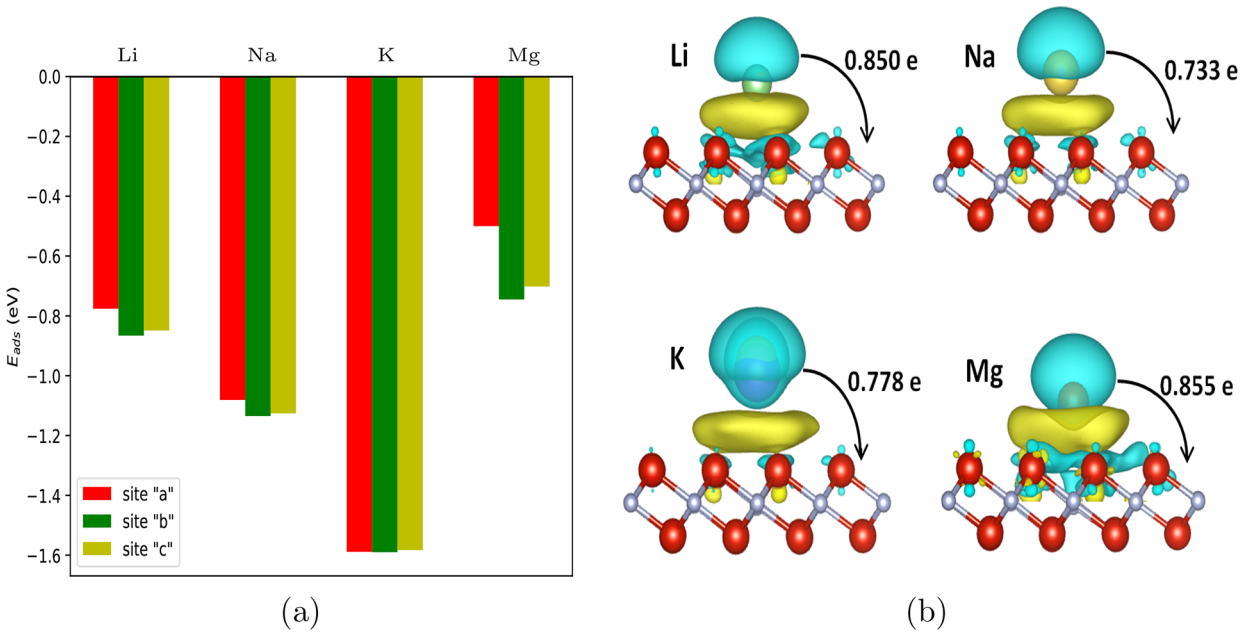

Figure 2. (a) Adsorption energies E_{ads} of Li, Na, K, and Mg atoms at different adsorption sites of V_2N monolayer. (b) Charge density difference of Li, Na, K, and Mg at the most stable adsorption site of V_2N monolayer. Yellow and blue colors with the isosurface value of 0.0010 e/Bohr^3 represent charge accumulation and depletion, respectively.

2. COMPUTATIONAL METHOD

The first-principles calculations are performed using the Vienna ab initio simulation package (VASP)[37,38] based on the density functional theory (DFT).[39,40] In the computations, valence wave functions are treated by projector augmented wave (PAW)[41] pseudopotential method. The plane-wave cutoff energy is 450 eV. The exchange-correlation function is described by the generalized gradient approximation (GGA) of the Perdew, Burke, and Ernzerhof (PBE) functional.[42] To correct the interactions between the adsorbed metal ions and the 2D electrode, the van der Waals (vdW) interaction is also included using the DFT-D3 method with Becke−Jonson damping[43,44] and is tested with the original vdW-DF[45] and "opt" functionals (optPBE-vdW).[46] For geometry optimization of unit cell, the Brillouin-zone (BZ) integration is performed using a regular Γ centered 16 × 16 × 1 k-mesh within Monkhorst−Pack scheme.[47] To avoid the spurious interactions, a vacuum space of more than 20 Å is used. The structural optimizations is performed by using the conjugate gradient method, and the convergence criterion is set to 1 × 10^{-5} eV/atom in energy and 0.01 eV/Å in force.

Here, a 4 × 4 × 1 supercell with one adsorbed metal atom is used to simulate adsorption and diffusion of the metal ions on V_2N monolayer. The diffusion energy barrier and minimum energy pathways of metal cation diffusion on the V_2N monolayer[48] are calculated with the climbing image nudged elastic band (CI-NEB) method. The force convergence criterion is less than 0.03 eV/Å in CI-NEB calculations.

3. RESULTS AND DISCUSSION

3.1. Structure and Electronic Properties of V_2N MXene Monolayer. In the crystal structure of V_2N MXene monolayer, the N atoms are sandwiched between the V(1)−V(2) bilayer forming an edge-shared V_6N octahedron as shown in Figure 1a. The optimized in-plane lattice constant of bulk V_2N is 2.904 Å, and the thickness of V_2N triple layers is 2.069 Å with V−N bond length of 1.970 Å. These values are well consistent with the previously reported theoretical results of V_2N.[49]

Next, the stability of V_2N MXene monolayer was examined by calculating its phonon dispersion as shown in Figure 1b. Near the Γ-point, the two in-plane acoustic phonons displayed linear dispersion, and the out-of-plane acoustic branch exhibited parabolic energy dispersion, presenting a typical phonon dispersion characteristic of 2D materials. No imaginary frequency is found in the considered Brillouin zone. Thus, the structure of V_2N MXene monolayer exhibits phonon stability. The calculated band structure and density of state of V_2N monolayer was also presented in Figure 1c. The energy band of V_2N monolayer crossing the Ferimi energy indicates its metallic behavior. The electrons near the Fermi energy that occupy mainly V-3d orbitals hybridized with seldom occupied N-2p orbitals. This metallic character of the V_2N monolayer makes it more competitive as an electrode material for LIBs and beyond, compared with the other 2D semconductors such as transition metal dichalcogenides.

3.2. Metal Atom Adsorption on the V_2N MXene Monolayer. In order to evaluate the electrochemical performance of V_2N monolayer, it is necessary to explore the preferred adsorption sites of these monovalent and multivalent metal atoms M (M = Li, Na, K, and Mg). In the V_2N MXene monolayer system, we considered three high symmetry adatom sites for metal atoms: top adsorption site "a", hcp adsorption site "b", and fcc adsorption site "c", as indicated in Figure 1a. The adsorption energy (E_{ads}) of a guest M atom on the V_2N monolayer is defined as

$$E_{ads} = (E_{total} - E_{V_2N} - cE_M)/c \quad (1)$$

where E_{total} and E_{V_2N} are the total energies of V_2N 4 × 4 × 1 supercell with and without adsorbed atoms, respectively. E_M is the chemical potential of the metal atom and is taken as the energy per one guest atom in its bulk phase. Here the hcp

https://doi.org/10.1021/acsomega.2c00936
ACS Omega 2022, 7, 17756−17764

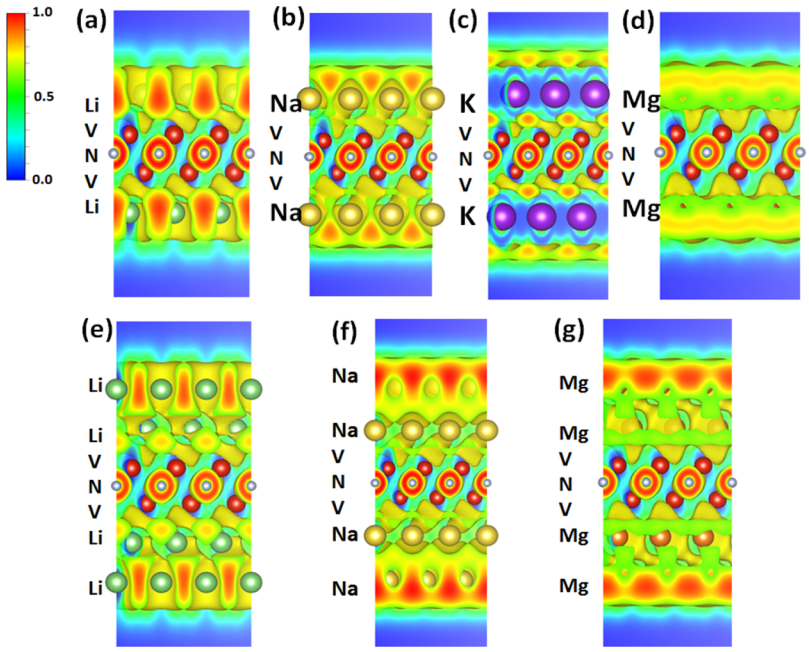

Figure 3. (a–d) Electron localization functions of (110) section for V_2NM_2 (M = Li, Na, K, and Mg). (e–g) Electron localization function isosurface (0.5) of the (110) section for V_2NM_4 (M = Li, Na, and Mg).

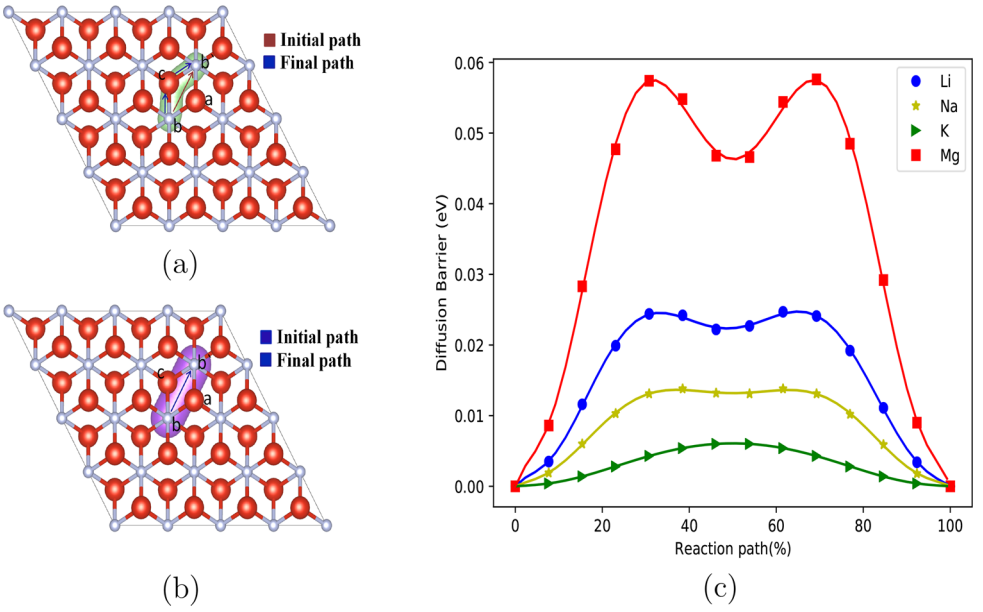

Figure 4. Initial and final ion diffusion paths for (a) Li, Na, and Mg. (b) K ions on the V_2N monolayer. (c) Diffusion barrier profiles of Li, Na, K, and Mg ions on the V_2N monolayer.

Bravais lattice structure for Mg and the bcc for Li, Na, and K are used for calculations as they are the most stable structures respectively at room temperatures and pressures. c is the number of the adsorbed atoms; here c = 1. The E_{ads} values of different guest atoms for the different adsorption sites of the V_2N monolayer are displayed in Figure 2a. It is found that all of the studied metal atoms can be effectively adsorbed on the V_2N monolayer as indicated by the negative E_{ads} values. The higher absolute value of E_{ads} suggests the stronger interaction between the guest metal atom and the V_2N monolayer. Overall, the investigated guest atom prefer to occupy the site "b" than the other two high symmetry positions "a" and "c". This may be caused by the larger electronegativity differences between the adsorbed atoms and the N atoms. Interesting for K atom, the E_{ads} values of the three sites are almost the same, which are also verified by its near zero diffusion barrier on V_2N monolayer.

Furthermore, to obtain an insight into the bonding of adsorption adatoms and V_2N monolayer, their charge transfer has been explored based on Bader charge analysis between the guest metal atoms and the monolayer V_2N.[50] The charge density difference (CDD) of the most stable adsorbed systems is shown in Figure 2b, defined as $\Delta\rho(r) = \rho_{total}(r) - \rho_{V2N}(r) - \rho_M(r)$. Herein, $\rho_{total}(r)$, $\rho_{V2N}(r)$, and $\rho_M(r)$ represent the charge densities of the total adsorption system, pristine V_2N, and one metal atom in the same lattice parameter, respectively.

https://doi.org/10.1021/acsomega.2c00936
ACS Omega 2022, 7, 17756–17764

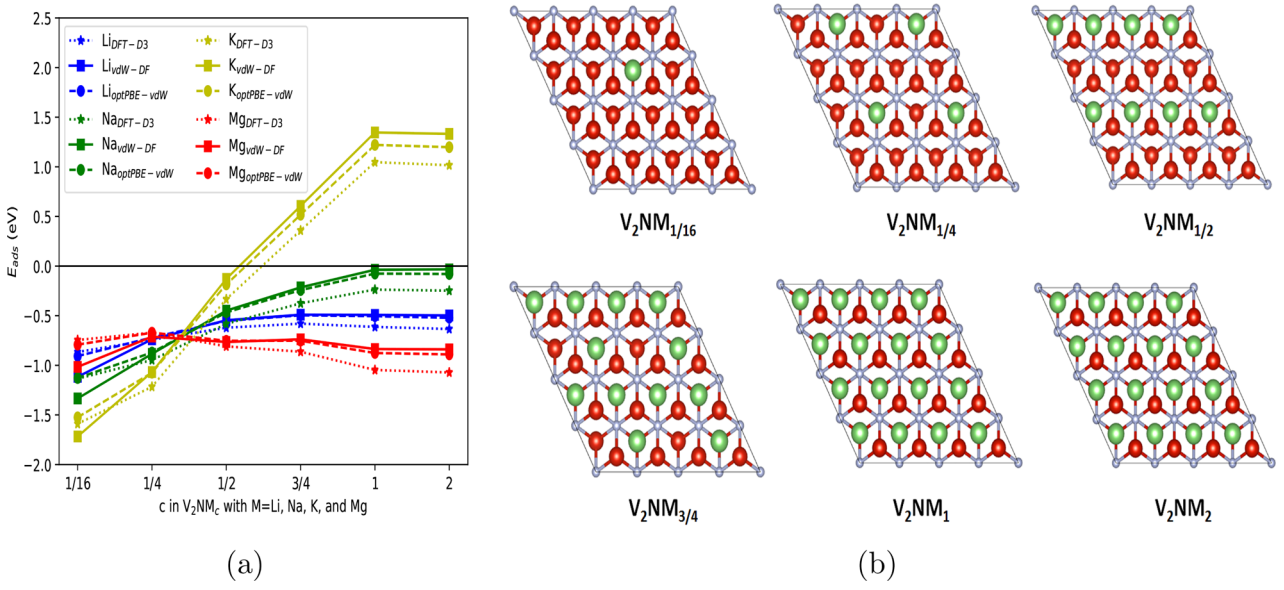

Figure 5. (a) Dependence of adsorption energies E_{ads} on c in V_2NM_c for different ions M, with c = 1/16, 1/4, 1/2, 3/4, 1, and 2; M = Li, Na, K, and Mg. The DTF-D3, vdW-DF, and optPBE-vdW represent three different methods to solved the vdW interaction. (b) Top view of V_2NM_c.

This CDD, as shown in Figure 2b, clearly visualizes the effect of adsorption on the charge distribution. From the CDD, the positive charge is mainly distributed on the metal ions. The Li, Na, K, and Mg atom can transfer 0.850, 0.733, 0.778, and 0.855 electrons, respectively, to V_2N monolayer. The charge transfer is related not only with the electronegativity difference but also the number of valence electrons of the adsorbed metal atoms.

To obtain a deeper insight into the adsorption behavior of metal ions, we also performed electron localization functions (ELF) to analyze the charge distributions of V_2N with one and two adsorption layers. Figure 3a–d shows the ELF of the (110) section for V_2NM_2 (M = Li, Na, K, and Mg). For Li, Na, and Mg, the electrons are spread out in the M layers forming a negative electron cloud (NEC). The NEC can screen the repulsion among the positive metal ions (M–M and M–V), so as to stabilize the adsorption layers.[51] By contrast, there are almost no NEC in the K layers of V_2NK_2, indicating that the electrons are more localized. Thus, this causes strong repulsion between the K ions and results in a positive E_{ads}. The screening effect can also be validated by the vertical distances between metal ions to V_2N monolayer. From Section 3.3, we know that K has the longest distance to reduce the repulsive interaction. Since Mg has two valence electrons compared with one for Li and Na, the screening effect of NEC is stronger in Mg than that in Li and Na. Therefore, Mg has the shortest distance, and Li and Na is in the middle. Figure 3e–g shows the ELF isosurface (0.5) of the (110) section for V_2NM_4 (M = Li, Na, and Mg). It is clear that both the second layer of Li, Na, and Mg are surrounded by NEC. However, there is almost no NEC in the first adsorption layer of Na. Thus, the V_2NNa_2 phase is unstable because of strong repulsive interaction, which results in the positive E_{ads} value of V_2NNa_4. The first layer of Li and Mg are surrounded by NEC, confirming the stable of two layers adsorption.

3.3. Ion Diffusion on the V_2N MXene Monolayer. The charge/discharge rate capability of rechargeable batteries is closely related to the mobility of cations on the electrodes. Thus, in this section we studied the energy barriers of adsorbed metal ions diffusion on the V_2N monolayer. As shown in Figure 2a, the most stable adsorption site is "b". Therefore, the diffusion path of metal ions on V_2N monolayer was designed between two neighboring most stable adsorption sites (b → b′). Here, 12 sampling points are equally and linearly separated on the pathway. The optimized diffusion paths and diffusion barrier profiles of different metal ions on V_2N monolayer are displayed in Figure 4. For Li, Na, and Mg ions, the calculated migration path is from one "b" site to the nearest "b′" site across a "c" site on top of V(2) atom in the third atomic layer (i.e., b → c → b′), which is two most stable adsorption sites via the metastable adsorption site "c". The calculated ion diffusion path is similar to diffusion path of Li ions on Ti_3C_2.[23] We can see that two saddle points correspond to the middle position of the b → c and the c → b′ bridges, and the local energy minimum of the profiles correspond to the metastable site "c". However, for K ions the final path is consistent with the initial path and a single saddle point is observed in the middle of the b → b′ bridge with almost zero diffusion barrier 0.004 eV which is also gained by almost the same adsorption energies of K at the three symmetry positions as showed in Figure 2a.

The diffusion energy barriers on V_2N monolayer are calculated in the ascending order: K < Na < Li < Mg ions, with 0.004 eV for K, 0.014 eV for Na, 0.025 eV for Li, and 0.058 eV for Mg ions, respectively. The Li diffusion barrier on V_2N is a little bit smaller than was reported by Pan.[49] Remarkably, compared with 0.33 eV on graphene[52] and 0.22 eV on VS_2,[53] Li ions have much lower diffusion energy barrier on V_2N, indicating faster transport and higher rate capability on V_2N monolayer. Other metal ions do also, which can also be used as high-rate electrode materials in rechargeable batteries. Although the binding energy of Na–V_2N system is stronger than that of the Li–V_2N system, Na has a lower diffusion energy barrier on V_2N monolayer than Li. The Na lower diffusion energy barrier may be related to its larger vertical distance of 2.60 Å, including the radius of the ion than that of Li ion 2.26 Å from the adsorption guest atom to V_2N monolayer. K ion does also, although K has the largest binding energy with V_2N monolayer; the diffusion barrier of K ion is

https://doi.org/10.1021/acsomega.2c00936
ACS Omega 2022, 7, 17756–17764

close to zero (~0.004 eV) with a vertical distance of 3.05 Å to V_2N monolayer. Additionally, Mg ion also shows a relatively larger binding energy with a relatively small adsorption distance of 2.12 Å. The Mg ion diffusion energy barrier of ~0.058 eV is still very low for the reported 2D energy storage materials. These analyses showed that 2D V_2N is a promising candidate for high rate electrode material because of low energy barrier of metal ions diffusion.

3.4. Storage Capacity and Open Circuit Voltage of the V_2N MXene Monolayer. The specific capacity and working voltage of electrode materials are two important parameters in rechargeable ion batteries. Here, we utilized a 4 × 4 × 1 supercell of V_2N monolayer to investigate the storage capacity. The charge−discharge process of V_2N can be described as the following half-cell reaction

$$V_2N + cM^{x+} + cxe^- \leftrightarrow V_2NM_c \quad (2)$$

where x is the valence state of the metal ions (x = 1 for M = Li, Na, K ions, and x = 2 for M = Mg ion). To estimate the maximum storage capacity of different metal ions on V_2N monolayer, we first calculated the evolution of adsorption energy (E_{ads}) per metal atom with the increased concentration of adsorbed ions.

We explored a series of adsorption configurations with chemical formula V_2NM_c by placing different number of metal ions on 2D monolayer, where c = 1/16, 1/4, 1/2, 3/4, 1, and 2 were defined as the number of M ions per chemical formula V_2N. The larger c demonstrates the higher coverage of the M ions on 2D V_2N, as displayed in Figure 5b. Although the stable cation-adsorption site "b" was found in a 4 × 4 × 1 supercell cell, the other two high symmetry sites "a" and "c" with the increased coverage are also investigated because the enhanced cation−cation interaction may lead to the migration of metal ions. The calculations showed that Li, K, and Mg prefer to staying at the site "c" when $c \geq 1/2$, which is different from one metal cation in a supercell. Na still prefers the site "b" with the increased coverage. The absorbed atoms of c = 2 represent that both sides of V_2N monolayer are fully covered by the metal ions. Figure 5a shows the dependence of E_{ads} on c in V_2NM_c for different ions. It can be seen that E_{ads} gradually increases with the increase of adsorbed metal ions because of the enhanced repulsion among metal ions. However, this trend is not obvious for Li and Na when $c \geq 1/2$, especially for Mg, and E_{ads} decreases a little. This may be due to the slight impact of repulsion caused by the relatively smaller ionic radius comparing to K ions. To ensure the accuracy of calculation, we also employed two methods of nonlocal correlation functional and "opt" functional that approximately accounts for dispersion interactions. As displayed in Figure 5a, the trend is roughly the same with a little different of the binding energy. Obviously, for the first adsorption layer of both sides by Li, Na, and Mg ions on V_2N monolayer, the calculated E_{ads} is −0.634, −0.248, and −1.073 eV, respectively, which is energetically stable, ensuring the feasibility of bilateral adsorption. However, the positive E_{ads} value of 0.359 eV for K ions indicates that the adsorption is unstable when c is larger than 1/2 because of the strong repulsive interaction caused by the relatively larger ionic radius. It should be noted that the higher storage capacity could be obtained through multilayer adsorption. Recently, double Na-atomic layers were observed in one interlayer of the fully intercalated sample.[54] Hence, we also considered bilayer adsorption through layer by layer adsorption of metal ions. For the second adsorption layer, three high symmetry sites including "a", "b", and "c", were all studied based on the first layer adsorption of metal ions on both sides of 2D V_2N at the most favorable sites.

For the second layer, Mg ions show a negative E_{ads} (−0.295 eV) indicating the stable bilayer adsorption. Li ions show a slightly negative E_{ads} (−0.009 eV), however, the value is comparable to that of the electrode material Ca_2N on which adsorption energy of Na is about −0.003 eV,[55] implying the practicability of bilayer adsorption. But it is unstable for Na bilayer adsorption because of a positive E_{ads} (0.276 eV). So, the maximum number of adsorbed metal ions are c = 4 for Li and Mg, c = 2 for Na, and c = 0.5 for K, respectively. In order to further confirm the stability of the maximum adsorbed configuration, we also calculated their phonon spectra. Except for $V_2NK_{0.5}$, no imaginary frequency was found at any wavevector for V_2NLi_4, V_2NMg_4, V_2NNa_2, and $V_2NK_{0.25}$, indicating the dynamically stable of those maximum adsorbed configurations.

We considered bilayer adsorption of both sides (c = 4) for Li and Mg ions, and one-layer adsorption of both sides (c = 2) for Na ions. Only partial-layer adsorption was taken into consideration for K ions (c = 0.25). So the estimated theoretical specific capacities are 925, 463, 58, and 1850 mAh/g for Li, Na, K, and Mg ions, respectively. Significantly, the theoretical capacity for Li is much higher than that of the conventional graphite anode used in Li-ion batteries. Despite of the same adsorption layers, the calculated capacity of multivalent Mg ions is obviously larger than that of Li ions because it can carry two valence electrons per atom.

Next, we estimated the average of OCV which is another key parameter to characterize the output voltage of rechargeable batteries. The electronic potential during the charge/discharge process can be determined by change in Gibbs free energy of the system, which is approximately equal to the difference in total energies before and after guest atoms adsorption.[18] The expression is described as

$$OCV = (E_{V_2N} + cE_M - E_{V_2NM_c})/cxe \quad (3)$$

where E_{V_2N}, $E_{V_2NM_c}$ and E_M are the total energy of V_2N, V_2NM_c and bulk metal M (M = Li, Na, K or Mg), respectively. c and x represent the number and valence state of the adsorbed metal ions, respectively. As analyzed above, the maximum number of adsorbed ions are c = 4 for V_2NLi_4/V_2NMg_4, c = 2 for V_2NNa_2, and c = 0.25 for $V_2NK_{0.25}$. Thus, the average OCVs of monolayer V_2N for Li, Na, K, and Mg ions can be calculated to be 0.32, 0.24, 1.22, and 0.34 V, respectively. It is found that the average OCV values are all positive and very low for V_2NLi_4, V_2NNa_2, and V_2NMg_4, further demonstrating that it is feasible of V_2N MXene monolayer as an anode material for rechargeable Li, Na and Mg ion batteries.$V_2NK_{0.25}$ shows a relatively higher average OCV. The exception may be due to the much stronger E_{ads} of K ion on V_2N monolayer and its lower K ions coverage.

3.5. Comparison to Other 2D electrodes. We compared V_2N monolayer with other 2D electrode materials about Li and Na ions diffusion barriers on these materials and their capacities.[27,51,53,55−62] Our predicted small theoretical diffusion barriers and high capacities for various monovalent and multivalent ions on V_2N MXene indicate that this nitride MXene is capable of high energy density and excellent rate capability in lithium-ion and beyond lithium-ion batteries. As is shown in Figure 6, the Li theoretical capacity of V_2N

https://doi.org/10.1021/acsomega.2c00936
ACS Omega 2022, 7, 17756−17764

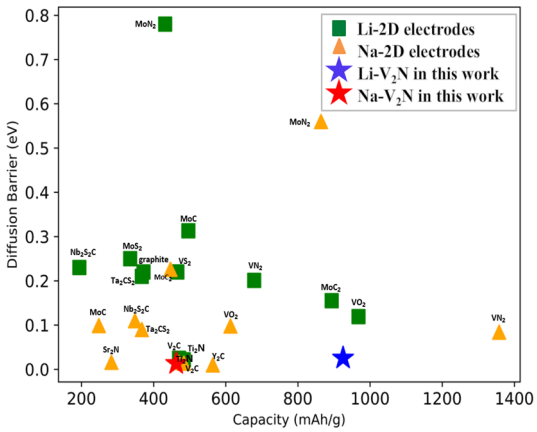

Figure 6. A comparison of V_2N monolayer with other 2D electrode materials: Li and Na ions diffusion barriers on these materials and their capacities.

monolayer is much higher than that of the commercialized anode material graphite and other 2D electrode materials, such as Ta_2CS_2, MoS_2, VS_2, Nb_2S_2C, MoC, MoN_2, and so on.[27,51,53,56−58,60,61] It is also found that the theoretical Li diffusion barrier on V_2N monolayer is quite small among these 2D electrode materials. For SIBs, the Na theoretical capacity of 463 mAh/g produced by V_2N monolayer is higher than that of Ta_2CS_2, MoC, MoC_2, Nb_2S_2C, and Sr_2N,[27,55−57] and also shows relative low theoretical diffusion barrier. Combined with the low average OCVs of 0.32 V for Li and 0.24 V for Na, V_2N monolayer exhibits superior electrochemical performance as a promising candidate for the anode materials of rechargeable Li and Na ion batteries.

4. CONCLUSIONS

We systematically investigated the physical properties and the electrochemical performances of 2D V_2N MXene monolayer using first-principles calculations. We found that V_2N MXene monolayer is not only dynamically stable but also exhibits metallic behavior. The diffusion barriers of these metal ions (M = Li, Na, Mg) on V_2N monolayer are rather low (<0.06 eV). The theoretical specific capacities of V_2N monolayer are as high as 925, 463, and 1850 mAh/g for Li, Na and Mg ions, respectively. Furthermore, the average OCVs of V_2N monolayer for Li, Na and Mg ions can be calculated to be 0.32, 0.24, and 0.34 V. All of these calculating results indicate that this nitride MXene V_2N can be used as a high-performance anode material for lithium-ion batteries and beyond.

AUTHOR INFORMATION

Corresponding Author

Yongmao Cai − *School of Science, Northeast Electric Power University, Jilin 132012, China;* orcid.org/0000-0001-9374-1120; Email: ymcai@neepu.edu.cn, 20132480@neepu.edu.cn

Authors

Hongli Liu − *School of Science, Northeast Electric Power University, Jilin 132012, China*

Zhendong Guo − *School of Science, Northeast Electric Power University, Jilin 132012, China*

Jing Zhou − *School of Chemical Engineering, Northeast Electric Power University, Jilin 132012, China*

Complete contact information is available at: https://pubs.acs.org/10.1021/acsomega.2c00936

Notes

The authors declare no competing financial interest.

ACKNOWLEDGMENTS

This work is supported by the National Natural Science Foundation of China (52172185) and the Project of Education Department of Jilin Province(JJKH20210084KJ), and authors also thank the Jilin Provincial Key Laboratory of Energy Big Data Analysis and Smart Computing for providing the HPC computing resources.

REFERENCES

(1) Yoshino, A. The Birth of the Lithium-Ion Battery. *Angew. Chem., Int. Ed.* **2012**, *51*, 5798−5800.
(2) Tarascon, J. M.; Armand, M. Issues and challenges facing rechargeable lithium batteries. *Nature* **2001**, *414*, 359−367.
(3) Goodenough, J. B.; Park, K. S. The Li-Ion Rechargeable Battery: A Perspective. *J. Am. Chem. Soc.* **2013**, *135*, 1167−1176.
(4) Tarascon, J. M. Is Lithium the New Gold? *Nat. Chem.* **2010**, *2*, 510−511.
(5) Slater, M. D.; Kim, D.; Lee, E.; Johnson, C. S. Sodium-ion batteries. *Adv. Funct. Mater.* **2013**, *23*, 947−958.
(6) Rajagopalan, R.; Tang, Y.; Ji, X.; Jia, C.; Wang, H. Advancements and Challenges in Potassium Ion Batteries: A Comprehensive Review. *Adv. Funct. Mater.* **2020**, *30*, 1909486.
(7) Song, M.; Niu, J.; Gao, H.; Kou, T.; Wang, Z.; Zhang, Z. Phase engineering in lead-bismuth system for advanced magnesium ion batteries. *J. Mater. Chem. A* **2020**, *8*, 13572−13584.
(8) Aurbach, D.; Lu, Z.; Schechter, A.; Gofer, Y.; Gizbar, H.; Turgeman, R.; Cohen, Y.; Moshkovich, M.; Levi, E. Prototype systems for rechargeable magnesium batteries. *Nature* **2000**, *407*, 724−727.
(9) Liu, Y.; Merinov, B. V.; Goddard, W. A. Origin of low sodium capacity in graphite and generally weak substrate binding of Na and Mg among alkali and alkaline earth metals. *Proc. Natl. Acad. Sci. U. S. A.* **2016**, *113*, 3735−3739.
(10) Divincenzo, D. P.; Mele, E. J. Cohesion and structure in stage-1 graphite intercalation compounds. *Phys. Rev. B* **1985**, *32*, 2538−2553.
(11) Wang, Z.; Shao, G. High-capacity cathodes for magnesium lithium chlorine tri-ion batteries through chloride intercalation in layered MoS_2: a computational study. *J. Mater. Chem. A* **2018**, *6*, 6830−6839.
(12) Levi, E.; Gofer, Y; Aurbach, D. On the Way to Rechargeable Mg Batteries: The Challenge of New Cathode Materials†. *Chem. Mater.* **2010**, *22*, 860−868.
(13) Ju, J.; Ma, J.; Wang, Y.; Cui, Y.; Han, P.; Cui, G. Solid-state energy storage devices based on two-dimensional nano-materials. *Energy Stor. Mater.* **2019**, *20*, 269−290.
(14) Jing, Y.; Zhou, Z.; Cabrera, C. R.; Chen, Z. Graphene, inorganic graphene analogs and their composites for lithium ion batteries. *J. Mater. Chem. A* **2014**, *2*, 12104−12122.
(15) Li, Y.; Wu, D.; Zhou, Z.; Cabrera, C. R.; Chen, Z. Enhanced Li Adsorption and Diffusion on MoS_2 Zigzag Nanoribbons by Edge Effects: A Computational Study. *J. Phys. Chem. Lett.* **2012**, *3*, 2221−2227.
(16) Pang, J.; Mendes, R. G.; Bachmatiuk, A.; Zhao, L.; Ta, H. Q.; Gemming, T.; Liu, H.; Liu, Z.; Rummeli, M. H. Applications of 2D MXenes in energy conversion and storage systems. *Chem. Soc. Rev.* **2019**, *48*, 72−133.
(17) Anasori, B.; Lukatskaya, M. R.; Gogotsi, Y. 2D metal carbides and nitrides (MXenes) for energy storage. *Nat. Rev. Mater.* **2017**, *2*, 16098.

(18) Er, D.; Li, J.; Naguib, M.; Gogotsi, Y.; Shenoy, V. B. Ti_3C_2 MXene as a high capacity electrode material for metal (Li, Na, K, Ca) ion batteries. ACS Appl. *Mater. Interfaces* **2014**, *6*, 11173−11179.
(19) Mashtalir, O.; Naguib, M.; Mochalin, V. N.; Dall'Agnese, Y.; Heon, M.; Barsoum, M. W.; Gogotsi, Y. Intercalation and delamination of layered carbides and carbonitrides. *Nat. Commun.* **2013**, *4*, 1716.
(20) Lukatskaya, M. R.; Mashtalir, O.; Ren, C. E.; Dall'Agnese, Y.; Rozier, P.; Taberna, P. L.; Naguib, M.; Simon, P.; Barsoum, M. W.; Gogotsi, Y. Cation intercalation and high volumetric capacitance of two-dimensional titanium carbide. *Science* **2013**, *341*, 1502−1505.
(21) Naguib, M.; Kurtoglu, M.; Presser, V.; Lu, J.; Niu, J.; Heon, M.; Hultman, L.; Gogotsi, Y.; Barsoum, M. W. Two-dimensional nanocrystals produced by exfoliation of Ti_3AlC_2. *Adv. Mater.* **2011**, *23*, 4248−4253.
(22) Wang, H.-W.; Naguib, M.; Page, K.; Wesolowski, D. J.; Gogotsi, Y. Resolving the structure of $Ti_3C_2T_x$ mxenes through multilevel structural modeling of the atomic pair distribution function. *Chem. Mater.* **2016**, *28*, 349−359.
(23) Tang, Q.; Zhou, Z.; Shen, P. Are MXenes Promising Anode Materials for Li Ion Batteries? Computational Studies on Electronic Properties and Li Storage Capability of Ti_3C_2 and $Ti_3C_2X_2$ (X = F, OH). *Monolayer. J. Am. Chem. Soc.* **2012**, *134*, 16909−16916.
(24) Yu, T.; Zhao, Z.; Liu, L.; Zhang, S.; Xu, H.; Yang, G. TiC_3 monolayer with high specific capacity for sodium-ion batteries. *J. Am. Chem. Soc.* **2018**, *140*, 5962−5968.
(25) Kamysbayev, V.; Filatov, A. S.; Hu, H.; Rui, X.; Lagunas, F.; Wang, D.; Klie, R. F.; Talapin, D. V. Covalent surface modifications and superconductivity of two-dimensional metal carbide MXenes. *Science* **2020**, *369*, 979−983.
(26) Seredych, M.; Shuck, C. E.; Pinto, D.; Alhabeb, M.; Precetti, E.; Deysher, G.; Anasori, B.; Kurra, N.; Gogotsi, Y. High-Temperature Behavior and Surface Chemistry of Carbide MXenes Studied by Thermal Analysis. *Chem. Mater.* **2019**, *31*, 3324−3332.
(27) Wu, M.; Xin, B.; Yang, W.; Li, B.; Dong, H.; Cheng, Y.; Wang, W.; Lu, F.; Wang, W.-H.; Liu, H. Metallic Monolayer Ta_2CS_2: An Anode Candidate for Li^+, Na^+, K^+, and Ca^{2+} Ion Batteries. *ACS Appl. Energy Mater.* **2020**, *3*, 10695−10701.
(28) Urbankowski, P.; Anasori, B.; Makaryan, T.; Er, D.; Kota, S.; Walsh, P. L.; Zhao, M.; Shenoy, V. B.; Barsoum, M. W.; Gogotsi, Y. Synthesis of two-dimensional titanium nitride Ti_4N_3(MXene). *Nanoscale* **2016**, *8*, 11385−11391.
(29) Soundiraraju, B.; George, B. K. Two-Dimensional Titanium Nitride (Ti_2N) MXene: Synthesis, Characterization, and Potential Application as Surface-Enhanced Raman Scattering Substrate. *ACS Nano* **2017**, *11*, 8892−8900.
(30) Venkateshalu, S.; Cherusseri, J.; Karnan, M.; Kumar, K. S.; Kollu, P.; Sathish, M.; Thomas, J.; Jeong, S. K.; Grace, A. N. New Method for the Synthesis of 2D Vanadium Nitride (MXene) and Its Application as a Supercapacitor Electrode. *ACS omega* **2020**, *5*, 17983−17992.
(31) Xiao, X.; Yu, H.; Jin, H.; Wu, M.; Fang, Y.; Sun, J.; Hu, Z.; Li, T.; Wu, J.; Huang, L.; Gogotsi, Y.; Zhou, J.; et al. Salt-Templated Synthesis of 2D Metallic MoN and Other Nitrides. *ACS Nano* **2017**, *11*, 2180−2186.
(32) Urbankowski, P.; Anasori, B.; Hantanasirisakul, K.; Yang, L.; Zhang, L.; Haines, B.; May, S. J.; Billinge, S. J.; Gogotsi, Y. 2D molybdenum and vanadium nitrides synthesized by ammoniation of 2D transition metal carbides (MXenes). *Nanoscale* **2017**, *9*, 17722−17730.
(33) Zhong, Y.; Xia, X.; Shi, F.; Zhan, J.; Tu, J.; Fan, H. J. Transition Metal Carbides and Nitrides in Energy Storage and Conversion. *Adv. Sci.* **2016**, *3*, 1500286.
(34) Liu, Y.; Jiang, Y.; Hu, Z.; Peng, J.; Lai, W.; Wu, D.; Zuo, S.; Zhang, J.; Chen, B.; Dai, Z.; Yang, Y.; Huang, Y.; Zhang, W.; Zhao, W.; Zhang, W.; Wang, L.; Chou, S.; et al. In-Situ Electrochemically Activated Surface Vanadium Valence in V_2C MXene to Achieve High Capacity and Superior Rate Performance for Zn-Ion Batteries. *Adv. Funct. Mater.* **2021**, *31*, 2008033.
(35) Zhang, X.; Zhang, Z.; Yao, S.; Chen, A.; Zhao, X.; Zhou, Z. An effective method to screen sodium-based layered materials for sodium ion batteries. *npj Comput. Mater.* **2018**, *4*, 13.
(36) Zhang, Z.; Zhang, X.; Zhao, X.; Yao, S.; Chen, A.; Zhou, Z. Computational screening of layered materials for multivalent ion batteries. *ACS omega* **2019**, *4*, 7822−7828.
(37) Kresse, G.; Furthmüller, J. Efficiency of ab-initio total energy calculations for metals and semiconductors using a plane-wave basis set. *Comput. Mater. Sci.* **1996**, *6*, 15−50.
(38) Kresse, G.; Furthmüller, J. Efficient Iterative Schemes for Ab Initio Total-Energy Calculations Using a Plane-Wave Basis Set. *Phys. Rev. B* **1996**, *54*, 11169−11186.
(39) Hohenberg, P.; Kohn, W. Inhomogeneous electron gas. *Phys. Rev.* **1964**, *136*, B864.
(40) Kohn, W.; Sham, L. J. Self-consistent equations including exchange and correlation effects. *Phys. Rev.* **1965**, *140*, A1133.
(41) Blochl, P. E. Projector augmented-wave method. *Phys. Rev. B* **1994**, *50*, 17953−17979.
(42) Perdew, J. P.; Burke, K.; Ernzerhof, M. Generalized gradient approximation made simple. *Phys. Rev. Lett.* **1996**, *77*, 3865−3868.
(43) Grimme, S.; Antony, J.; Ehrlich, S.; Krieg, H. A consistent and accurate ab initio parametrization of density functional dispersion correction (DFT-D) for the 94 elements H-Pu. *J. Chem. Phys.* **2010**, *132*, 154104.
(44) Grimme, S.; Ehrlich, S.; Goerigk, L. Effect of the damping function in dispersion corrected density functional theory. *J. Comput. Chem.* **2011**, *32*, 1456−1465.
(45) Dion, M.; Rydberg, H.; Schröder, E.; Langreth, D. C.; Lundqvist, B. I. Van der Waals density functional for general geometries. *Phys. Rev. Lett.* **2004**, *92*, 246401.
(46) Klimeš, J.; Bowler, D. R.; Michaelides, A. Chemical accuracy for the van der Waals density functional. *J. Phys.: Condens. Matter* **2010**, *22*, 022201.
(47) Monkhorst, H. J.; Pack, J. D. Special points for Brillouin-zone integrations. *Phys. Rev. B* **1976**, *13*, 5188−5192.
(48) Henkelman, G.; Uberuaga, B. P.; Jónsson, H. A climbing image nudged elastic band method for finding saddle points and minimum energy paths. *J. Chem. Phys.* **2000**, *113*, 9901−9904.
(49) Pan, H. Electronic properties and lithium storage capacities of two-dimensional transition-metal nitride monolayers. *J. Mater. Chem. A* **2015**, *3*, 21486−21493.
(50) Henkelman, G.; Arnaldsson, A.; Jónsson, H. A fast and robust algorithm for Bader decomposition of charge density. *Comput. Mater. Sci.* **2006**, *36*, 354−360.
(51) Wang, D.; Gao, Y.; Liu, Y.; Jin, D.; Gogotsi, Y.; Meng, X.; Du, F.; Chen, G.; Wei, Y. First-principles calculations of Ti_2N and Ti_2NT_2 (T= O, F, OH) monolayers as potential anode materials for lithium-ion batteries and beyond. *J. Phys. Chem. C* **2017**, *121*, 13025−13034.
(52) Uthaisar, C.; Barone, V. Edge effects on the characteristics of li diffusion in graphene. *Nano Lett.* **2010**, *10*, 2838−2842.
(53) Jing, Y.; Zhou, Z.; Cabrera, C. R.; Chen, Z. Metallic VS_2 Monolayer: A Promising 2D Anode Material for Lithium Ion Batteries. *J. Phys. Chem. C* **2013**, *117*, 25409−25413.
(54) Wang, X.; Shen, X.; Gao, Y.; Wang, Z.; Yu, R.; Chen, L. Atomic-Scale Recognition of Surface Structure and Intercalation Mechanism of Ti_3C_2X. *J. Am. Chem. Soc.* **2015**, *137*, 2715−2721.
(55) Hu, J.; Xu, B.; Yang, S. A.; Guan, S.; Ouyang, C.; Yao, Y. 2D Electrides as Promising Anode Materials for Na-Ion Batteries from First-Principles Study. *ACS Appl. Mater. Interfaces* **2015**, *7*, 24016−24022.
(56) Jing, Y.; Liu, J.; Zhou, Z.; Zhang, J.; Li, Y. Metallic Nb_2S_2C Monolayer: A Promising Two-Dimensional Anode Material for Metal Ion Batteries. *J. Phys. Chem. C* **2019**, *123*, 26803−26811.
(57) Yu, Y.; Guo, Z.; Peng, Q.; Zhou, J.; Sun, Z. Novel two-dimensional molybdenum carbides as high capacity anodes for lithium/sodium-ion batteries. *J. Mater. Chem. A* **2019**, *7*, 12145−12153.
(58) Zhang, X.; Yu, Z.; Wang, S.-S.; Guan, S.; Yang, H. Y.; Yao, Y.; Yang, S. A. Theoretical prediction of MoN_2 monolayer as a high

https://doi.org/10.1021/acsomega.2c00936
ACS Omega 2022, 7, 17756−17764

capacity electrode material for metal ion batteries. *J. Mater. Chem. A* **2016**, *4*, 15224−15231.
(59) Wang, Y.; Song, N.; Song, X.; Zhang, T.; Zhang, Q.; Li, M. Metallic VO_2 monolayer as an anode material for Li, Na, K, Mg or Ca ion storage: a first-principle study. *RSC Adv.* **2018**, *8*, 10848−10854.
(60) Li, Y.-M.; Guo, Y.-L.; Jiao, Z.-Y. The effect of S-functionalized and vacancies on V_2C MXenes as anode materials for Na-ion and Li-ion batteries. *Curr. Appl. Phys.* **2020**, *20*, 310−319.
(61) Dong, Y.; Tang, Z.; Liang, P.; Wan, H.; Wang, H.; Wang, L.; Shu, H.; Chao, D. 2D-VN_2 MXene as a novel anode material for Li, Na and K ion batteries: Insights from the first-principles calculations. *J. Colloid Interface Sci.* **2021**, *593*, 51−58.
(62) Hou, J.; Tu, K.; Chen, Z. Two-Dimensional Y_2C Electride: A Promising Anode Material for Na-Ion Batteries. *J. Phys. Chem. C* **2016**, *120*, 18473−18478.

https://doi.org/10.1021/acsomega.2c00936
ACS Omega 2022, 7, 17756−17764